Energy Engineering

Tech Science Press

Doi:10.32604/ee.2025.061172

ARTICLE

# Optimal Evaluation of Photovoltaic Consumption Schemes in Distribution Networks Based on BASS Model for Photovoltaic Installed Capacity Prediction

**Chenyang Fu***, **Xinghua Wang**, **Zilv Li**, **Xixian Liu**, **Xiongfei Zhang and Zhuoli Zhao**

School of Automation, Guangdong University of Technology, Guangzhou, 510000, China

*Corresponding Author: Chenyang Fu. Email: 2112204491@mail2.gdut.edu.cn

Received: 18 November 2024; Accepted: 04 March 2025; Published: 25 April 2025

**ABSTRACT:** With the large-scale promotion of distributed photovoltaics, new challenges have emerged in the photovoltaic consumption within distribution networks. Traditional photovoltaic consumption schemes have primarily focused on static analysis. However, as the scale of photovoltaic power generation devices grows and the methods of integration diversify, a single consumption scheme is no longer sufficient to meet the actual needs of current distribution networks. Therefore, this paper proposes an optimal evaluation method for photovoltaic consumption schemes based on BASS model predictions of installed capacity, aiming to provide an effective tool for generating and evaluating photovoltaic consumption schemes in distribution networks. First, the BASS diffusion model, combined with existing photovoltaic capacity data and roof area information, is used to predict the trends in photovoltaic installed capacity for each substation area, providing a scientific basis for consumption evaluation. Secondly, an improved random scenario simulation method is proposed for assessing the photovoltaic consumption capacity in distribution networks. This method generates photovoltaic integration schemes based on the diffusion probabilities of different regions and evaluates the consumption capacity of each scheme. Finally, the Technique for Order Preference by Similarity to an Ideal Solution (TOPSIS) is used to comprehensively evaluate the generated schemes, ensuring that the selected scheme not only meets the consumption requirements but also offers high economic benefits and reliability. The effectiveness and feasibility of the proposed method are validated through simulations of the IEEE 33-node system, providing strong support for optimizing photovoltaic consumption schemes in distribution networks.

**KEYWORDS:** BASS model; photovoltaic installation forecast; diffusion probability; photovoltaic consumption; multi objective evaluation

## 1 Introduction

With the continuous growth of global energy demand and increasing concerns about carbon emissions, renewable energy has gradually become an important alternative to traditional fossil fuels. Photovoltaic (PV) power generation, due to its cleanliness, renewability, and distributed nature, is gaining widespread adoption globally [1–3]. By the end of 2021, China's newly installed PV capacity reached 54.88 million kW [4]. However, the large-scale integration of distributed photovoltaics can cause voltage fluctuations, making the assessment of the consumption capacity of distribution networks with high levels of PV integration particularly important [5–7]. Predicting the future installed capacity of photovoltaics in distribution networks is a prerequisite for the evaluation of their consumption capacity.

Literature [8,9] addressed the issue of PV growth in the evaluation of photovoltaic installed capacity by adopting an increase in penetration rate, which does not accurately reflect the actual growth of photovoltaics.

Therefore, more realistic predictions of PV capacity growth are needed. Some recent studies have focused on predicting future trends in distributed PV capacity. For example, literature [10] utilized a system dynamics model based on an improved grey wolf optimization algorithm to forecast user PV installations, incorporating factors such as electricity subsidies that directly affect household PV sales. In a similar vein, literature [11] proposed a system dynamics model to predict incentives for PV installation and decision-making models for users regarding grid-connected PV systems. However, both studies focused on objective factors such as dynamic policy evolution, rather than simulating the subjective factors of user purchasing behavior, which limits their accuracy in photovoltaic forecasting. If both subjective and objective factors are considered comprehensively, the prediction of photovoltaic installed capacity can be more accurate.

Currently, methods for assessing PV consumption capacity can be broadly classified into two categories: software simulation methods [12–14] and mathematical optimization algorithms [15–17]. Software simulation methods, such as those using MATLAB and other computational software, build systems for simulation, allowing for real-time calculation and evaluation of various parameters. Literature [12] employs a two-stage adjustable robust optimization to address the uncertainties in load demands and DG outputs, and proposes a robust comprehensive DG capacity assessment method considering three-phase power flow modeling and active network management (ANM) techniques. Literature [13] discussed the photovoltaic consumption capacity under three different scenarios: concentrated at the feeder source, middle point, and end point, and determined the maximum consumption capacity for each location. The second category is mathematical optimization algorithms, including analytical methods, intelligent optimization algorithms, and stochastic scenario simulations, which establish network models and solve them using various algorithms. For instance, literature [15] categorized PV integration into single, multiple, or all nodes and applied an improved simulated annealing-particle swarm optimization algorithm to find the maximum consumption capacity for different distribution network conditions. However, the results obtained from analytical methods and intelligent optimization algorithms are often local or global optima, which may not reflect the true, comprehensive photovoltaic consumption capacity of the distribution network. By using stochastic scenario simulation methods, various photovoltaic integration situations can be simulated, and extensive simulation sampling can be conducted to reflect the actual consumption capacity of the distribution network.

This paper adopts the BASS diffusion model to predict the future growth of distributed photovoltaics in each substation area. Secondly, a photovoltaic integration scenario generation method based on diffusion probabilities is proposed, which simulates photovoltaic integration schemes and evaluates the consumption capacity of all schemes year by year as photovoltaic capacity grows [18]. Finally, the Technique for Order Preference by Similarity to an Ideal Solution (TOPSIS) [19] is applied, which not only evaluates the scheme with the highest maximum photovoltaic consumption capacity under optimal economic efficiency and reliability but also provides the corresponding photovoltaic configuration. Using the IEEE 33-bus system as a benchmark example, simulations are conducted in MATLAB, and the results validate the accuracy and effectiveness of the proposed method.

## 2 Prediction of Distributed Photovoltaic Installed Capacity Based on the BASS Diffusion Model

The consumption capacity of distributed photovoltaics is influenced by the location of connection substations, the size of rooftop areas, and the progress of development. On one hand, it is necessary to select a tool to simulate the diffusion process, ensuring that the growth of photovoltaics aligns with actual conditions; on the other hand, a development cap needs to be established to constrain growth based on rooftop photovoltaic area.

Building on this, the approximate assessment of photovoltaic installed capacity in distribution networks can illustrate the dynamic evaluation process of annual growth and provide a clear representation of the photovoltaic consumption situation for each year. The Bass Diffusion Model is commonly used to predict the diffusion trends of innovative products and technologies, and it has also been widely applied in the prediction of rooftop photovoltaic installed capacity [20]. The basic form of the BASS diffusion model is as follows:

$$n_t = \frac{dN_t}{dt} = p\left(M - N_t\right) + q\frac{1}{M}N_t\left(M - N_t\right) \tag{1}$$

In the equation, $n_t$ represents the installed capacity of distributed photovoltaics at time $t$; $N_t$ denotes the cumulative purchased capacity of distributed photovoltaics; $M$ indicates the installation potential of distributed photovoltaics; $p$ represents the innovation coefficient; and $q$ denotes the imitation coefficient, $p, q \in [0, 1]$.

The diffusion parameters $M$, $p$ and $q$ of the BASS diffusion model have a significant impact on prediction accuracy. This study uses nonlinear least squares to estimate the values of the diffusion parameters $p$ and $q$. The installation potential $M$ is influenced by the rooftop area of substations; therefore, the data for this study is sourced from the measurement of rooftop areas obtained from high-resolution satellite imagery [21]. The basic prediction results are shown in Fig. 1.

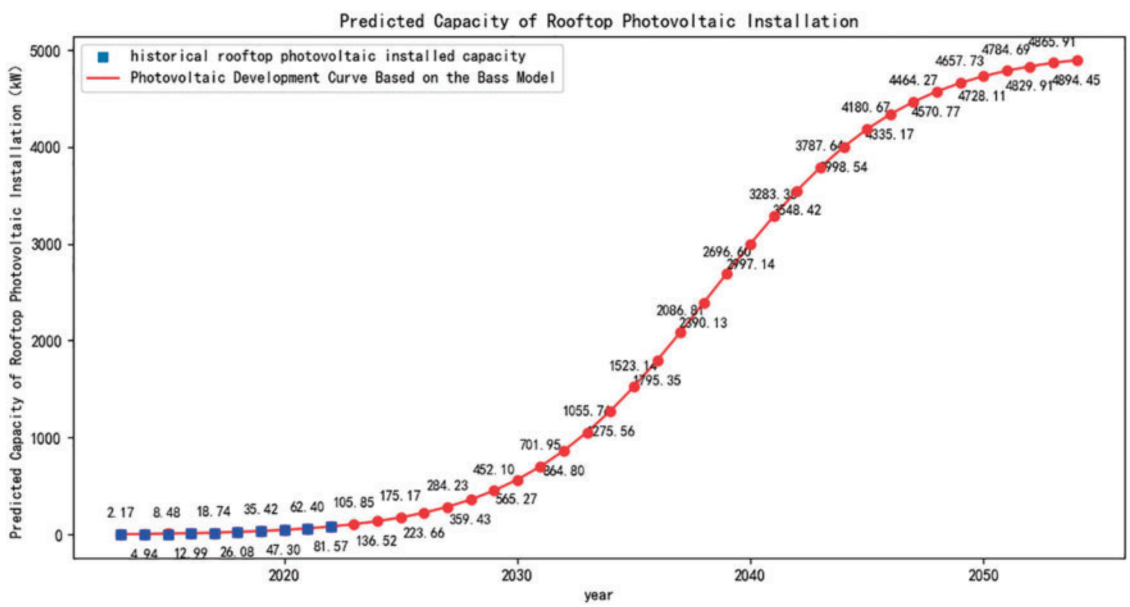


**Figure 1:** BASS diffusion model distributed photovoltaic installation fitting diagram

The blue squares represent historical rooftop photovoltaic data from 2013 to 2022, while the red circles indicate the photovoltaic installed capacity values predicted based on the BASS model. The overall prediction curve exhibits an S-shaped pattern. In the early stages, the growth is primarily influenced by the innovation coefficient $p$, resulting in a gradual increase from 2023 to 2030. In the later stages, the influence of the imitation coefficient $q$ becomes dominant, leading to a rapid increase in the mid-term, followed by a slowdown as it approaches saturation from 2030 to 2055. The saturation value is determined by the installation potential $M$, with the installed capacity in 2055 reaching 4894.45 kW, which is close to the figure of 4900 kW depicted in the graph. Overall, the trend aligns with the initial rapid growth of photovoltaics followed by gradual saturation and slowing growth, effectively predicting the true trajectory of photovoltaic development and demonstrating the validity of the BASS diffusion model. However, in practice, the rooftop photovoltaic area of substations is dynamically changing, so for the prediction process, a certain amount of new rooftop photovoltaic area will be added for the upcoming year to introduce uncertainty, thereby simulating this variation to make the predictions more reflective of reality.

## 3 Based on the Improved Stochastic Scenario Simulation Method for Photovoltaic Consumption Capacity Assessment in Distribution Networks

Large-scale integration of distributed photovoltaics may lead to unstable power fluctuations and frequency deviations in the grid, affecting power quality. In severe cases, it can cause reverse power flow issues, potentially resulting in equipment damage or failure, and even triggering system collapse. This paper focuses on the issue of voltage fluctuations by imposing limits on the maximum voltage to facilitate bounded simulations. There is uncertainty in the integration of distributed photovoltaics in substations, influenced by users' subjective factors. Therefore, this paper adopts a photovoltaic integration scheme generation method based on diffusion parameters, which maintains uncertainty while making the integration choices more realistic. Subsequently, based on the photovoltaic forecasts for each substation area, the photovoltaic growth for all schemes is evaluated under typical load scenarios, thereby providing an approximate assessment of the consumption capacity for each scheme.

### *3.1 Generation of Typical Scenarios*

The load demand of the distribution network and the output of distributed photovoltaics exhibit significant temporal characteristics and fluctuations. This study selects the most common photovoltaic-load scenarios for evaluation. Based on annual load data and solar radiation intensity data, the K-means clustering method is utilized to identify the day with the most typical photovoltaic load variation. The load-photovoltaic difference is then defined as the moment when the absolute value of the load and the photovoltaic output have the greatest disparity, which is analyzed as a typical moment. The formula is as follows:

$$\alpha_{PV}(t) = P_{load}(t) - P_{pv}(t) \tag{2}$$

In the formula, $\alpha_{PV}(t)$ represents the load-photovoltaic difference, indicating the disparity between the absolute value of photovoltaic output and the absolute value of load at time $t$. The moment when this difference reaches its minimum is defined as the typical moment $T$. $P_{pv}(t)$ and $P_{load}(t)$ represent the photovoltaic output and active power values of the distribution network at time $t$, respectively. Most existing literature employs the moment with the maximum photovoltaic-load ratio as the typical time slice; however, this approach can lead to the misselection of extreme cases, adversely affecting subsequent research (for instance, when photovoltaic output is low but load active power approaches zero). In this study, we adopt the condition of selecting the minimum load-photovoltaic difference, which helps avoid such extreme cases and accurately identifies common moments where photovoltaic output is high and load is low.

### *3.2 Stochastic Scenario Simulation of Photovoltaic Consumption Schemes in Distribution Networks Based on Diffusion Probabilities*

#### *3.2.1 Stochastic Scenario Simulation Method Based on Diffusion Probabilities*

Since the integration of distributed photovoltaics is not only random but also has a certain degree of subjectivity, using Monte Carlo fully random sampling or uniform sampling methods to simulate distributed photovoltaic access schemes is not accurate. In the previous section, the BASS diffusion model was used to predict photovoltaic installed capacity, resulting in three diffusion parameters ($M$, $p$ and $q$) for each substation area. Therefore, this paper proposes a probability sampling method based on diffusion parameters, distinguishing between different user and load types to make the random simulation process more aligned with engineering practices. During the simulation of photovoltaic installed capacity prediction, the diffusion probability involves changes over time and the growth of installed capacity, primarily influenced by the imitation coefficient $q$. Thus, the sampling probability calculation formula for substation areas is as follows:

$$P\left(i\right)=\alpha_1 M+\alpha_2\frac{q_1}{n_{t1}p_1+q_1}+\alpha_3\frac{q_2}{n_{t2}p_2+q_2} \tag{3}$$

In the formula, $P$ represents the sampling probability value for the substation area; $i$ represents the substation number; and $\alpha_1, \alpha_2, \alpha_3$ represent the weight coefficients; $M$ is the photovoltaic installation potential from the BASS diffusion model; $p_1, q_1$ and $p_2, q_2$ represent the innovation coefficient and imitation coefficient of the BASS model before and after the addition of new rooftop area; $n_{t1}$ and $n_{t2}$ represent the distributed photovoltaic installation capacities at moments before $t_2$ and after $t_1$ the addition of rooftops.

### *3.2.2 Improved Stochastic Scenario Simulation Steps*

After determining the typical time slice $T$, random simulations can be conducted for the distribution network. The specific steps for simulating photovoltaic access schemes are as follows:

(1) **Determine the number of photovoltaic access nodes.** Let the total number of nodes in the distribution network be $N$, excluding generator nodes. From the remaining load nodes $N_{load}=N-1$, the number of randomly generated photovoltaic nodes is $N_{pv}\left(0<N_{pv}\le N_{load}\right)$, resulting in a photovoltaic access position set of size $W_{PV}=\left\{W_1, W_2, \ldots, W_{N_{load}}\right\}$.

(2) **Determine the photovoltaic access locations.** Based on the access quantity, randomly select $N_{pv}$ elements from set $W_{PV}$ according to the diffusion probability, resulting in a combination of positions $w_{PV}=\left\{W_1, W_2, \ldots, W_{N_{pv}}\right\}$.

(3) **Incremental capacity growth of each photovoltaic node.** Each selected photovoltaic node will increase its capacity annually according to the predicted future photovoltaic installed capacity for each substation area, and the total installed capacity will be recorded after each increment.

(4) **Power flow calculation.** Calculate the power flow results for this consumption scheme year by year, recording voltage data for each year, and determine whether the voltage at each substation meets the voltage constraints.

$$U_i \le U_{\max} \tag{4}$$

where $U_i$ is the voltage value at node $i$ and $U_{\max}$ is the rated maximum operating voltage.

(5) **Repeat steps (1) and (2).** Multiple photovoltaic access schemes can be randomly generated, saving the access locations, total installed capacity, and voltage results for each scheme.

## *3.3 Photovoltaic Consumption Capacity Assessment in Distribution Networks*

This paper uses the voltage level of the distribution network and photovoltaic capacity limits as the main criteria for approximate evaluation, analyzing the consumption capacity under different distributed photovoltaic access schemes. Fig. 2 shows the scatter plot of the photovoltaic consumption capacity assessment for a distribution network, generated after the Monte Carlo sampling of photovoltaic access schemes. Each "line" in the figure represents a unique random photovoltaic access scheme, indicated by different colors. Based on the BASS diffusion model, the future photovoltaic access capacity for each substation area was predicted, allowing the total photovoltaic access capacity to increase annually according to the forecasted values, resulting in the scattered points on the "line". Each point on a "line" represents the maximum voltage value of the distribution network and the total photovoltaic access capacity for a given access scheme in different years. The horizontal axis indicates the total photovoltaic access capacity of the random access schemes, while the vertical axis represents the maximum system voltage for each random scheme at different access capacities. A vertical comparison shows significant differences in voltage levels among the schemes at the same photovoltaic access capacity, highlighting the importance of studying the site selection and configuration of photovoltaics in distribution networks.

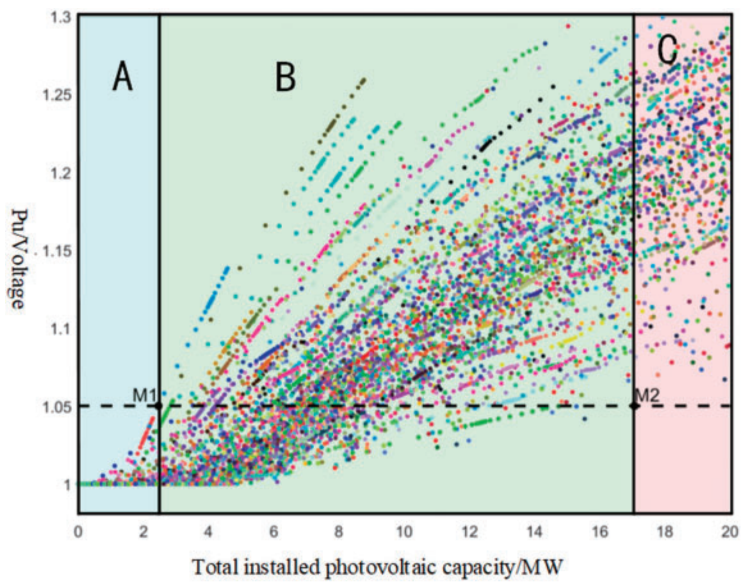


**Figure 2:** Simulation results of photovoltaic random access scheme

In Fig. 2, the dashed line at a voltage of 1.05 pu represents the voltage constraint of the distribution network. The intersections formed between the voltage constraint dashed line and the various "lines" indicate several points of interest. The labeled intersection points $M1$ and $M2$ represent the approximate minimum and maximum photovoltaic access capacities, respectively. The simulation results are divided into three regions, denoted as $A$, $B$, $C$, based on the horizontal coordinates $x_1$ and $x_2$ of points $M1$ and $M2$.

The area to the left of the horizontal coordinate $x_1$ of point $M1$ is referred to as Region $A$. The scattered points in this area indicate that, regardless of the total photovoltaic capacity being below this threshold, the distribution network can absorb the power without exceeding the voltage limits, regardless of the access locations and quantities.

The area greater than $x_1$ and less than $x_2$ is referred to as Region $B$. The scattered points in this area suggest that the number and location of photovoltaic connections significantly impact the voltage levels. Therefore, it is necessary to plan the photovoltaic configuration rationally to effectively avoid voltage violations.

The area greater than $x_2$ is referred to as Region $C$. In this region, the total photovoltaic capacity is relatively high, and any access configuration will lead to voltage violations. Reasonable planning solutions are needed to address the absorption issues related to photovoltaic output.

The scheme near point $M2$ in area $B$ is the target scheme, and the photovoltaic access scheme at this point represents the photovoltaic configuration scenario under the maximum photovoltaic consumption capacity of the distribution network. However, as can be seen from the figure, using Monte Carlo sampling results in fewer schemes near point $M2$ in the target area $B$, with a large difference in the capacities of the available alternative consumption schemes, making it difficult to perform a comprehensive optimization. The probability sampling method based on diffusion parameters can make the generated random schemes more concentrated near points, making the approximate maximum absorption capacity of candidate schemes close.

## 4 Comprehensive Selection of Photovoltaic Consumption Schemes Based on TOPSIS

In the $B$ region, although the photovoltaic access schemes near point $M2$ have similar photovoltaic access capacities, there are significant differences in the number of photovoltaic connections and their locations across the various schemes. To ensure the economic efficiency and reliability of the distribution network with distributed photovoltaic access, this section comprehensively selects the candidate schemes based on three indicators: voltage quality, annual investment costs, and total photovoltaic capacity.

### *4.1 Voltage Quality Model*

Good voltage quality is essential for the stable operation of power systems and the normal functioning of equipment. This paper uses the level exceeding the upper voltage constraint as an evaluation metric and establishes a voltage deviation model to assess the voltage quality of photovoltaic access schemes.

$$f_1(i) = \begin{cases} \frac{U_{\max} - \max(U_i(t))}{U_{\max} - U_{\min}}, & \max(U_i(t)) > U_{\max} \\ 0, & \max(U_i(t)) \le U_{\min} \end{cases} \tag{5}$$

In the equation, $f_1(i)$ represents the voltage deviation value of the consumption scheme $i$; $U_{\max}$ and $U_{\min}$ are the upper and lower voltage limits of the distribution network system; and $\max(U_i(t))$ is the maximum voltage value at the node when the consumption scheme $i$ is connected at its maximum capacity.

### *4.2 Annual Investment Cost Model*

The initial investment for distributed photovoltaic (PV) integration mainly relates to the installation of inverters and PV modules. The mid-term costs primarily include the purchase costs of electricity from higher levels, while the later stage mainly involves the operation and maintenance (O&M) costs of PV generation. This paper establishes an investment cost model for distributed PV integration around these three indicators. The investment cost model for distributed PV is as follows:

$$f_2(i) = C_{inv} + C_{fee} + C_m \tag{6}$$

In the formula, $C_{inv}$ represents the initial investment cost of distributed photovoltaic integration, and $C_{fee}$ indicates the electricity purchase cost for the distribution network.

The formula for the initial investment cost of distributed PV integration is as follows:

$$C_{\text{inv}} = \lambda_0 + \lambda_1 \sum_{n=1}^{N} x_{DG} P_{DG}^n + \lambda_2 \sum_{n=1}^{N} x_{DG} P_{DG}^n \tag{7}$$

In the formula, $\lambda_0$ and $\lambda_1$ represent the fixed investment cost and unit capacity cost of the photovoltaic inverter, respectively. $x_{DG}$ is a binary variable, where $x_{DG} = 0$ indicates that distributed photovoltaic is not integrated at the $n$ node, and $x_{DG} = 1$ indicates that distributed photovoltaic is integrated at the $n$ node. $P_{DG}^n$ denotes the photovoltaic capacity connected at the $n$ node, while $\lambda_2$ represents the fixed investment cost of the photovoltaic modules. $N$ is the total number of nodes.

The formula for the higher-level electricity purchase costs is as follows:

$$C_{fee} = \lambda_3(t)_4 \sum_{t=1}^{8760} \sum_{n=1}^{N} x_{DG} \left(P_{load}^{n} - P_{DG}^{n}\right) \tag{8}$$

In the equation, $\lambda_3(t)$ represents the time-of-use electricity price for a given day; $P_{load}^{n}$ is the load power at node $n$.

Finally, the post-investment primarily consists of the operational and maintenance costs for the equipment, which can be expressed as:

$$C_m = \lambda_4 \sum_{t=1}^{8760} \sum_{n=1}^{N} x_{DG} P_{DG}^{n} \tag{9}$$

In the equation, $\lambda_4$ represents the unit operational and maintenance cost of the photovoltaic system.

### *4.3 Comprehensive Selection of Schemes Based on TOPSIS*

After determining the candidate consumption schemes and calculating the voltage deviation and investment costs for each scheme, this paper employs the TOPSIS method based on the entropy weighting approach to conduct a comprehensive evaluation of consumption capacity, voltage quality, and investment costs, thereby selecting the optimal consumption scheme. The TOPSIS method [22], also known as the Technique for Order of Preference by Similarity to Ideal Solution, is a multi-attribute decision-making method used to assess the merits of alternative schemes. The entropy weighting method can better reflect the correlation among attributes and the uncertainty of their weights. The steps for selecting the optimal consumption scheme using the entropy-weighted TOPSIS method are as follows:

(1) Select $n$ candidate schemes based on the approximate evaluation results of the consumption capacity, which serve as the $n$ evaluation objects.

(2) Calculate the evaluation indicators for each object: total consumption capacity, voltage deviation, and investment cost. Establish the initial multi-objective matrix $X = \left(x_{ij}\right)_{3\times \mathrm{n}}$, and perform normalization on the result values to obtain the standardized multi-objective matrix.

$$z_{ij} = x_{ij} \Big/ \sqrt{\sum_{i=1}^{n} x_{ij}^{2}} \tag{10}$$

(3) Determine the entropy weights for each indicator. Calculate the probability matrix $p_{ij}$, information entropy $e_j$, and information utility values $d_j$ of the multi-objective matrix, and finally compute the entropy weights.

$$w_j = \frac{d_j}{\sum_{j=1}^{3} d_j} \tag{11}$$

(4) Calculate the positive and negative ideal solutions $Z^+$ and $Z^-$ for the evaluation indicators, and assess the distances between each evaluation object's indicators and the ideal solutions, denoted as $D_i^+$ and $D_i^-$.

$$\begin{cases} Z^+ = \left(z_{i1}^+, z_{i2}^+, z_{i3}^+\right) = \left(\max z_{i1}, \max z_{i2}, \max z_{i3}\right) \\ Z^- = \left(z_{i1}^-, z_{i2}^-, z_{i3}^-\right) = \left(\min z_{i1}, \min z_{i2}, \min z_{i3}\right) \end{cases} \tag{12}$$

$$\begin{cases} D_i^+ = \sqrt{\sum_{j=1}^{3} W_j \times \left(Z_j^+ - z_{ij}\right)^2}, i = 1, 2, \ldots, n \\ D_i^- = \sqrt{\sum_{j=1}^{-} W_j \times \left(Z_j^+ - z_{ij}\right)^2}, i = 1, 2, \ldots, n \end{cases} \tag{13}$$

(5) Calculate the proximity of each evaluation object to the ideal solution, resulting in a final score. Normalize the scores to rank the schemes and select the scheme with the maximum score as the optimal consumption scheme.

## 5 Example Analysis

### *5.1 Example Introduction*

This study uses the IEEE 33-node distribution network system for simulation, which is divided into four areas: commercial, industrial, residential, and mixed-use zones. The network topology is shown in Fig. 3. The system operates at a voltage level of 12.66 kV, with a base power of 10 MVA and voltage limits set at 1.05 and 0.95 pu. The total system power is 3.175 MW + 2.3 MVar, with node 1 serving as the balancing node, set at a voltage of 1.0 pu, while the remaining 32 nodes are load nodes capable of integrating photovoltaic systems. The residential area includes nodes 1 to 13, represented in green; the mixed-use area consists of nodes 14 to 18, shown in gray; the commercial area encompasses nodes 19 to 25, depicted in blue; and the industrial area includes nodes 26 to 33, illustrated in orange.

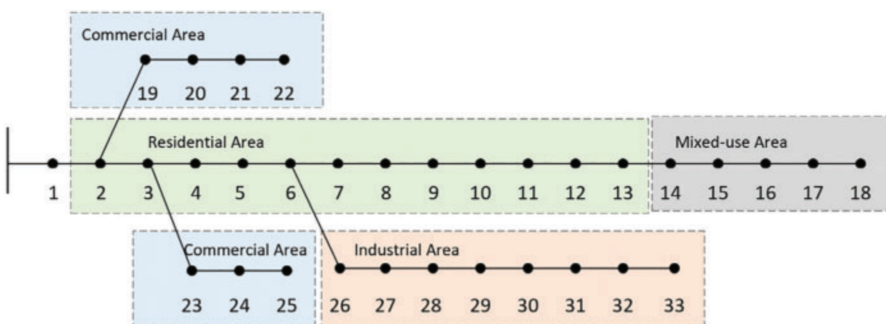


**Figure 3:** IEEE 33 node distribution network system topology diagram

The photovoltaic capacity estimation for the IEEE 33-node system is conducted by region. Since 2013, the National Energy Administration has published annual data on distributed photovoltaic installed capacity nationwide. The parameters for the Bass diffusion model in this study are derived from the distributed photovoltaic installed capacity data spanning a decade from 2013 to 2022, predicting the future photovoltaic capacity for each area from 2023 to 2055 over the next 33 years. However, the total photovoltaic area will change with urban development. To simulate this incremental change, different areas will see varying total rooftop area increases in different years, as detailed in Table 1. This approach provides a more realistic capacity forecast, ultimately yielding the predicted results for the 33 areas, with a specific area's prediction illustrated in Fig. 4. In the figure, the blue squares represent historical photovoltaic installed capacity data, while the red curve is the fitted curve of the future photovoltaic installed capacity for each year, showing the trend of photovoltaic capacity changes in the region.

**Table 1:** Newly added rooftop area for photovoltaics in various regions

| Substation type | New rooftop area/m$^2$ | Year of new rooftop |
|---|---|---|
| **Residential area** | 500 | 2050 |
| **Commercial area** | 1000 | 2044 |
| **Industrial area** | 1000 | 2040 |
| **Mixed-use area** | 750 | 2048 |

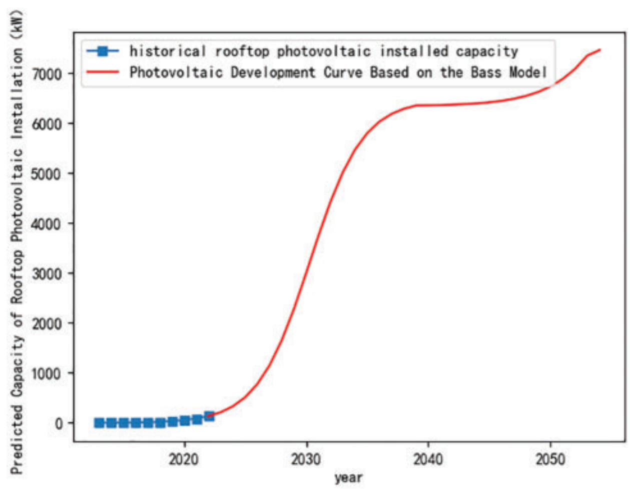


**Figure 4:** Forecast of distributed photovoltaic installed capacity in a certain district

After reviewing the data, the fixed investment cost for distributed photovoltaic modules is 6 ¥/W; the fixed investment cost and unit capacity cost for photovoltaic inverters are 805.85 yuan and 422 ¥/kW, respectively. The peak, valley, and flat electricity prices for purchased power are 0.904, 0.312, and 0.600 ¥/(kW·h). The unit operation and maintenance cost for distributed photovoltaic systems is 0.1 ¥/(kW·h). Data for solar radiation intensity and load from a city in China is selected, with the corresponding normalized values shown in Fig. 5, illustrating the variation in solar radiation intensity and load over the course of the year (365 days).

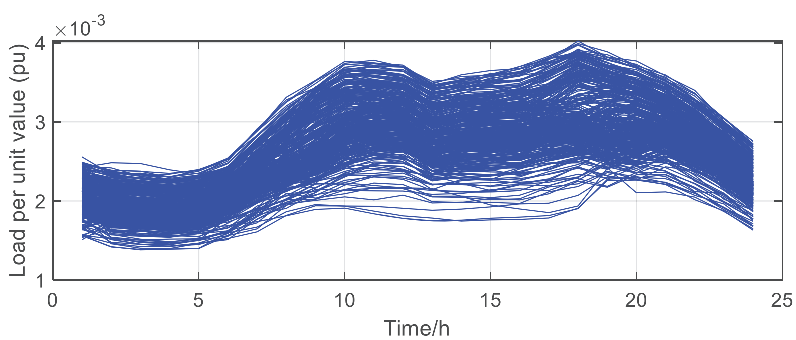


**Figure 5:** (Continued)

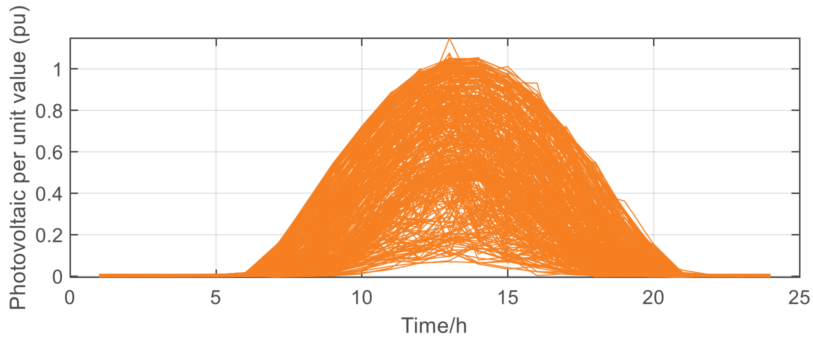


**Figure 5:** Light radiation intensity and load power per unit value

### 5.2 Example Simulation

Based on the annual solar radiation intensity and load data, K-means clustering was performed to identify a typical day that represents the most common combination of solar radiation and load throughout the year, as shown in Fig. 6. According to the method described in Section 3.1, the minimum load-solar radiation difference for the typical day is 0.2693, occurring at 14:00. This moment is designated as the typical time, with a normalized solar radiation intensity value of 0.5018 and a normalized load value of 0.7712.

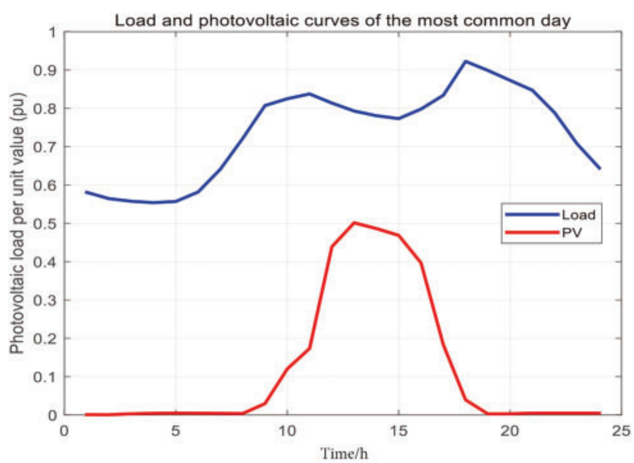


**Figure 6:** Typical solar radiation and load changes

At this typical time, random simulations of photovoltaic consumption schemes and approximate evaluations of consumption capacity were conducted following the methods outlined in Sections 3.2 and 3.3. First, the weight coefficients of the diffusion parameters were defined as 0.4, 0.3, and 0.3, which provided the sampling probabilities for each feeder node. Based on these diffusion probabilities, 1000 random samples were generated, resulting in 1000 random access schemes. The maximum normalized voltage values and total photovoltaic capacities for each scheme were recorded, as shown in Fig. 7. The approximate maximum consumption capacity for this distribution network system was determined to be 13.61416 MW, with the horizontal coordinates of M1 and M2 being 2.6597 and 14.5692 MW, respectively.

Compared to Fig. 2, the use of the diffusion probability-based sampling method resulted in a denser distribution of the generated random access schemes between $M1$ and $M2$. In Fig. 2, the schemes near

$M2$ were more sparse, leading to significant differences in the maximum photovoltaic capacities of the final candidate schemes. Fig. 7, in contrast to Fig. 2, shows a closer approximation, enhancing the sampling accuracy and concentrating the necessary "rays", thereby making the simulation results more effective.

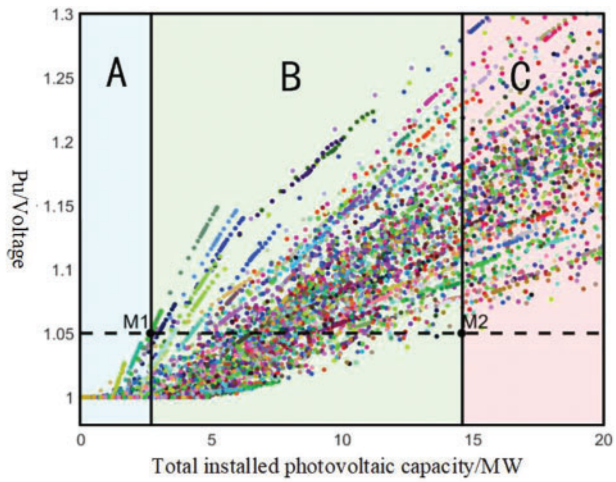


**Figure 7:** Simulation results of photovoltaic random access scheme

The maximum consumption capacities of the various schemes were ranked, and the top 10 capacity schemes were selected as candidates for evaluation. The scoring results are presented in descending order in Table 2.

**Table 2:** Newly added rooftop area for photovoltaics in various regions

| Scheme number | Final score | Voltage deviation $f_1(i)$ | Investment cost $f_2(i)$/¥10,000 | Total photovoltaic capacity $f_3(i)$/MW |
|---|---|---|---|---|
| 1 | 0.1973 | 0.1012 | 9617.73 | 12.48731 |
| 2 | 0.1801 | 0.1081 | 9294.35 | 12.13905 |
| 3 | 0.1267 | 0.1299 | 9084.71 | 11.81966 |
| 4 | 0.1245 | 0.133 | 9579.26 | 12.38495 |
| 5 | 0.1070 | 0.1370 | 9058.04 | 11.18827 |
| 6 | 0.0918 | 0.1582 | 10,147.0 | 13.61416 |
| 7 | 0.0741 | 0.1338 | 9569.82 | 12.34055 |
| 8 | 0.0491 | 0.1648 | 9349.99 | 12.20542 |
| 9 | 0.0283 | 0.1081 | 9181.07 | 11.87682 |
| 10 | 0.0211 | 0.2062 | 9143.85 | 11.86555 |

As shown in Table 2, the highest-scoring Scheme 1 has a score of 0.1973, making it the optimal photovoltaic consumption scheme when considering the comprehensive factors of consumption capacity, investment benefits, and voltage quality. Compared to Schemes 2 and 3, although Scheme 1 incurs higher investment costs, it can accommodate more photovoltaic capacity without exceeding voltage limits, while also maintaining a lower voltage deviation during continuous PV integration. The method presented in this paper enables the distribution network to maximize consumption with minimal investment under substantial distributed photovoltaic integration, while ensuring stable voltage quality.

The configuration of distributed photovoltaic integration for Scheme 1 is illustrated in Fig. 8. To validate the rationality of the scheme, it was tested under the most extreme scenario of the year, specifically at the moment when the solar load ratio is maximized, using annual operational data. The results are shown in Fig. 9.

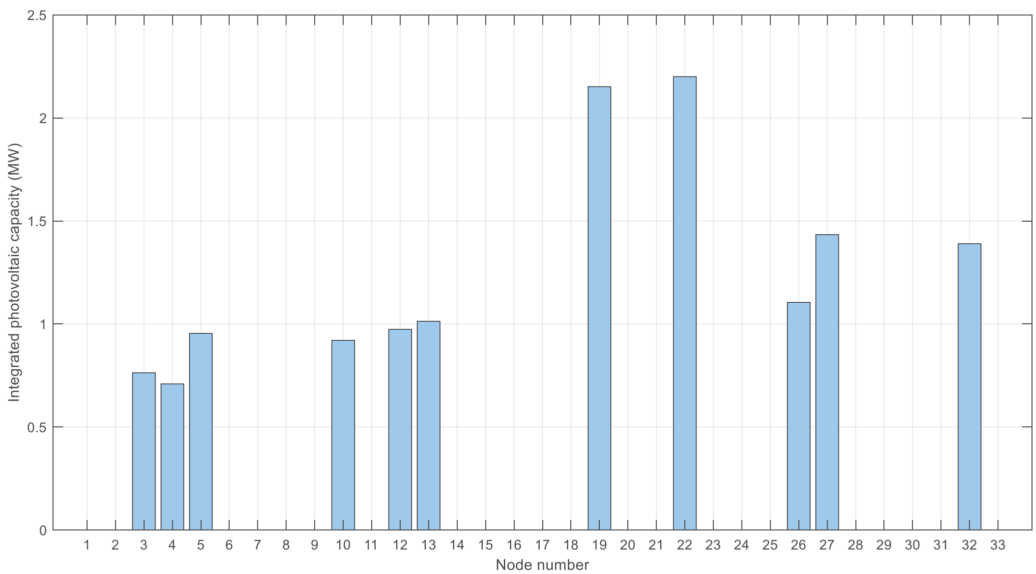


**Figure 8:** Optimal consumption plan for photovoltaic access configuration

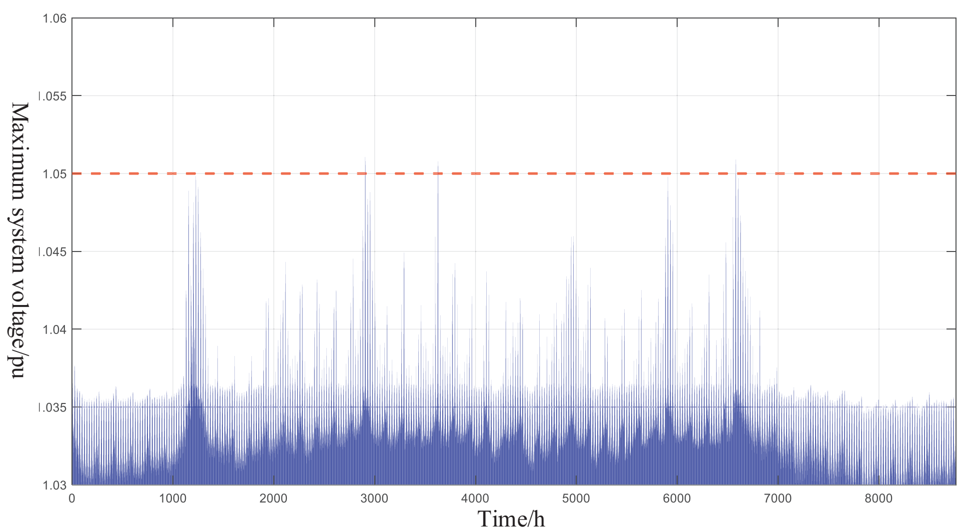


**Figure 9:** Voltage verification diagram based on annual operating data

As seen in Fig. 9, this integration scheme experiences voltage violations for 8 h during the extreme typical scenario within the annual operational cycle, with minimal violation levels. This indicates the representativeness of the selected typical moment and the rationality of the integration scheme.

Using the improved particle swarm optimization algorithm method from literature [15], this paper solves the example with the objectives of system consumption capacity, voltage deviation, and investment costs. The maximum photovoltaic consumption scheme configuration for the IEEE 33-node system is obtained, as illustrated in Fig. 10.

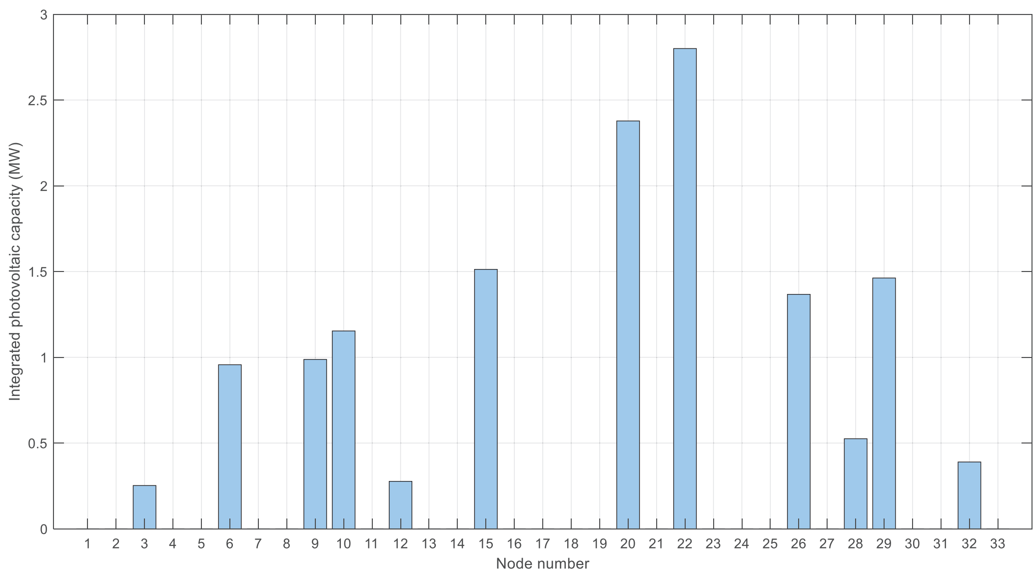


**Figure 10:** Mathematical optimization algorithm for maximum photovoltaic consumption and access configuration

As shown in this figure, the photovoltaic configuration scenarios obtained in reference [15] are nodes 3, 6, 9, 10, 12, 15, 20, 22, 26, 28, 29, and 32, with a total photovoltaic capacity of 13.89 MW. Although this is higher than the 12.48 MW result obtained by the method in this paper, the photovoltaic capacity at node 22 reaches 2.8001 MW, exceeding its rooftop area limit of 2.5035 MW, which does not comply with practical constraints. In addition, the consumption assessment method based on the improved particle swarm optimization not only fails to provide annual consumption evaluation results but also cannot simulate and compare various photovoltaic integration scenarios, thus failing to reflect the comprehensive photovoltaic consumption capacity of the distribution network. In contrast, the consumption assessment method based on the improved stochastic scenario simulation in this paper simulates various photovoltaic integration scenarios and conducts extensive simulation sampling to reflect the actual consumption capacity of the distribution network.

## 6 Conclusion

This study presents an evaluation method for optimizing photovoltaic consumption schemes in distribution networks based on BASS model predictions of installed PV capacity. The method aims to reasonably evaluate the photovoltaic consumption capacity of distribution networks under the considerations of economic efficiency and reliability. The research leads to the following conclusions:

(1) A method based on the BASS diffusion model predicts the future photovoltaic capacity of the distribution network. This approach incorporates both objective and subjective factors to forecast the development trend of photovoltaic installed capacity, ensuring that the predictions align with reality.
(2) A photovoltaic consumption evaluation method is proposed, which uses a photovoltaic random scenario method based on diffusion probabilities to generate photovoltaic access schemes and assess the consumption capacity of these schemes.
(3) The Technique for Order of Preference by Similarity to Ideal Solution (TOPSIS) method is used to evaluate the economic efficiency and reliability of the scheme with the maximum consumption capacity, making the final consumption scheme more reasonable and providing valuable reference for professionals.

In future assessments of the photovoltaic consumption capacity in distribution networks, additional factors such as the integration of solar energy and storage systems (solar-storage synergy), intelligent optimization scheduling, and further refinement of regional differences in consumption capacity should also be considered.

**Acknowledgement:** Thank you for the information provided by Guangdong Power Grid Co., Ltd.

**Funding Statement:** This work was supported in part by the The Planning Subject Project of Guangdong Power Grid Co., Ltd. (62273104).

**Author Contributions:** The authors confirm contribution to the paper as follows: study conception and design: Chenyang Fu and Xinghua Wang; data collection: Chenyang Fu and Zilv Li; analysis and interpretation of results: Chenyang Fu, Xixian Liu and Xiongfei Zhang; draft manuscript preparation: Chenyang Fu and Zhuoli Zhao. All authors reviewed the results and approved the final version of the manuscript.

**Availability of Data and Materials:** The data presented in this study are available on request from the corresponding author.

**Ethics Approval:** Not applicable.

**Conflicts of Interest:** The authors declare no conflicts of interest to report regarding the present study.

## Nomenclature

| | |
|---|---|
| $n_t$ | The installed capacity of distributed photovoltaics at time $t$ |
| $N_t$ | The cumulative purchased capacity of distributed photovoltaics |
| $M$ | The installation potential of distributed photovoltaics |
| $p$ | The innovation coefficient $p \in [0,1]$ |
| $q$ | Denotes the imitation coefficient $q \in [0,1]$ |
| $\alpha_{PV}(t)$ | The load-photovoltaic difference, indicating the disparity between the absolute value of photovoltaic output and the absolute value of load at time $t$ |
| $T$ | The moment when this difference reaches its minimum is defined as the typical moment |
| $P_{pv}(t)$ | The photovoltaic output of the distribution network at time $t$ |
| $P_{load}(t)$ | The active power values of the distribution network at time $t$ |
| $U_i$ | The voltage value at node $i$ |
| $U_{\max}$ | The rated maximum operating voltage |
| $U_{\min}$ | The lower voltage limits of the distribution network system |
| $P$ | The sampling probability value for the substation area |
| $i$ | Represents the substation number |
| $\alpha_i$ | The weight coefficients |

| | |
|---|---|
| $p_1, q_1$ | The innovation coefficient and imitation coefficient of the BASS model before the addition of new rooftop area |
| $p_2, q_2$ | The innovation coefficient and imitation coefficient of the BASS model after the addition of new rooftop area |
| $n_{t1}$ | The distributed photovoltaic installation capacities at moments before $t_2$ the addition of rooftops |
| $n_{t2}$ | The distributed photovoltaic installation capacities at moments after $t_1$ the addition of rooftops |
| $f_1(i)$ | The voltage deviation value of the consumption scheme $i$ |
| $\max(U_i(t))$ | The maximum voltage value at the node when the consumption scheme $i$ is connected at its maximum capacity |
| $C_{\text{inv}}$ | The initial investment cost of distributed photovoltaic integration |
| $C_{fee}$ | The electricity purchase cost for the distribution network |
| $\lambda_0$ | The fixed investment cost of the photovoltaic inverter |
| $\lambda_1$ | The unit capacity cost of the photovoltaic inverter |
| $x_{DG}$ | A binary variable, where $x_{DG} = 0$ indicates that distributed photovoltaic is not integrated at the $n$ node, and $x_{DG} = 1$ indicates that distributed photovoltaic is integrated at the $n$ node |
| $P_{DG}^n$ | The photovoltaic capacity connected at the $n$ node |
| $N$ | The total number of nodes |
| $\lambda_3(t)$ | The time-of-use electricity price for a given day |
| $P_{load}^n$ | The load power at node $n$ |
| $\lambda_4$ | The unit operational and maintenance cost of the photovoltaic system |

## References

1. Li J, Chen S, Wu Y, Wang Q, Liu X, Qi L, et al. How to make better use of intermittent and variable energy? A review of wind and photovoltaic power consumption in China. Renew Sustain Energy Rev. 2021;137:110626. doi:10.1016/j.rser.2020.110626.
2. Fan Q, Weng J, Liu D. Low-carbon economic operation of integrated energy systems in consideration of demand-side management and carbon trading. Front Energy Res. 2023;11:1230878. doi:10.3389/fenrg.2023.1230878.
3. Peng L, Mauzerall DL, Zhong YD, He G. Heterogeneous effects of battery storage deployment strategies on decarbonization of provincial power systems in China. Nat Commun. 2023;14(1):4858. doi:10.1038/s41467-023-40337-3.
4. van der Meer DW, Widén J, Munkhammar J. Review on probabilistic forecasting of photovoltaic power production and electricity consumption. Renew Sustain Energy Rev. 2018;81(1):1484–512. doi:10.1016/j.rser.2017.05.212.
5. Zheng Z, Hong B, Yin G, Zhu J. Relative merit of improving network hosting capacity for renewable generation. In: Proceedings of the International Conference on Renewable Power Generation (RPG); 2015 Oct 17–18; Beijing, China. p. 1–4. doi:10.1049/cp.2015.0409.
6. Mi Y, Liu C, Yang J, Liu Z, Zhu H, Wang T. Evaluation method of renewable energy accommodation considering wind-solar correlation. In: 2021 4th International Conference on Energy, Electrical and Power Engineering (CEEPE); 2021 Apr 23–25; Chongqing, China. p. 1205–09. doi:10.1109/CEEPE51765.2021.9475722.
7. Al-Saadi H, Zivanovic R, Al-Sarawi SF. Probabilistic hosting capacity for active distribution networks. IEEE Trans Ind Inform. 2017;13(5):2519–32. doi:10.1109/TII.2017.2698505.
8. Farag HE, El Saadany EF, El Chaar L. A multilayer control framework for distribution systems with high DG penetration. In: 2011 International Conference on Innovations in Information Technology; 2011 Apr 25–27; Abu Dhabi, United Arab Emirates. p. 94–9. doi:10.1109/INNOVATIONS.2011.5893877.
9. Aziz T, Ketjoy N. PV penetration limits in low voltage networks and voltage variations. IEEE Access. 2017;5:16784–792. doi:10.1109/ACCESS.2017.2747086.
10. Argüello A, Lara JD, Rojas JD, Valverde G. Impact of rooftop PV integration in distribution systems considering socioeconomic factors. IEEE Syst J. 2017;12(4):3531–42. doi:10.1109/JSYST.2017.2739022.
11. Hsu CW. Using a system dynamics model to assess the effects of capital subsidies and feed-in tariffs on solar PV installations. Appl Energy. 2012;100(4):205–17. doi:10.1016/j.apenergy.2012.02.039.

12. Chen X, Wu WC, Zhang BM. Robust capacity Assessment on Global of distributed generation in unbalanced distribution networks incorporating ANM techniques. IEEE Trans Sustain Energy. 2018;9(2):651–63. doi:10.1109/TSTE.2017.2754421.
13. Hoke A, Butler R, Hambrick J, Kroposki B. Steady-state analysis of maximum photovoltaic penetration levels on typical distribution feeders. IEEE Trans Sustain Energy. 2013;4(2):350–7. doi:10.1109/TSTE.2012.2225115.
14. Lamedica R, Geri A, Gatta FM, Sangiovanni S, Maccioni M, Ruvio A. Integrating electric vehicles in microgrids: overview on hosting capacity and new controls. IEEE Trans Ind Appl. 2019;55(6):7338–46. doi:10.1109/TIA.2019.2933800.
15. Chen S, Zhang Y, Zheng J. Assessment on global urban photovoltaic carrying capacity and adjustment of photovoltaic spatial planning. Sustainability. 2021;13(6):3149. doi:10.3390/su13063149.
16. Han C, Lee D, Song S, Jang G. Probabilistic assessment of PV hosting capacity under coordinated voltage regulation in unbalanced active distribution networks. IEEE Access. 2022;10:35578–88. doi:10.1109/ACCESS.2022.3163595.
17. Koirala A, Van Acker T, D'hulst R, Van Hertem D. Hosting capacity of photovoltaic systems in low voltage distribution systems: a benchmark of deterministic and stochastic approaches. Renew Sustain Energy Rev. 2022;155(1):111899. doi:10.1016/j.rser.2021.111899.
18. Zavvar E, Pinto TF, Santos RP. Identification of probability distributions of SCFs in three-planar KT-joints. Ocean Eng. 2024;312(P3):119222. doi:10.1016/j.oceaneng.2024.119222.
19. Ding F, Mather B. On distributed PV hosting capacity estimation, sensitivity study, and improvement. IEEE Trans Sustain Energy. 2016;8(3):1010–20. doi:10.1109/TSTE.2016.2640239.
20. Zhang X, Li H, Liu Q, Tan X. A study on the technology diffusion of China's solar photovoltaic based on bass and generalized bass model. In: 2020 5th International Conference on Materials Science, Energy Technology and Environmental Engineering; 2020 Aug 7–9; Shanghai, China; 2020. Vol. 571. p.012016. doi:10.1088/1755-1315/571/1/012016.
21. Chen X, Cui W, He J, Wu Z, Liu Y, Peng X. Evaluation of photovoltaic utilization potential of urban building roof. In: 2023 6th International Conference on Energy, Electrical and Power Engineering (CEEPE); 2023 May 12–14; Guangzhou, China. p. 1017–22. doi:10.1109/CEEPE58418.2023.10165705.
22. Huang JW, Chen R, Wang XX, Zhou YH. Study on the application of fuzzy TOPSIS to the multi-objective decision making. In: 2010 International Conference on Intelligent Computation Technology and Automation; 2010 May 11–12; Changsha, China. p. 560–3. doi:10.1109/ICICTA.2010.226.